SPECIAL ISSUE ARTICLE

Optimization of an Electron Transport Layer to Enhance the Power Conversion Efficiency of Flexible Inverted Organic Solar Cells

Kang Hyuck Lee · Brijesh Kumar ·
Hye-Jeong Park · Sang-Woo Kim

Abstract The photovoltaic (PV) performance of flexible inverted organic solar cells (IOSCs) with an active layer consisting of a blend of poly(3-hexylthiophene) and [6, 6]-phenyl C_{61}-butlyric acid methyl ester was investigated by varying the thicknesses of ZnO seed layers and introducing ZnO nanorods (NRs). A ZnO seed layer or ZnO NRs grown on the seed layer were used as an electron transport layer and pathway to optimize PV performance. ZnO seed layers were deposited using spin coating at 3,000 rpm for 30 s onto indium tin oxide (ITO)-coated polyethersulphone (PES) substrates. The ZnO NRs were grown using an aqueous solution method at a low temperature (90°C). The optimized device with ZnO NRs exhibited a threefold increase in PV performance compared with that of a device consisting of a ZnO seed layer without ZnO NRs. Flexible IOSCs fabricated using ZnO NRs with improved PV performance may pave the way for the development of PV devices with larger interface areas for effective exciton dissociation and continuous carrier transport paths.

Keywords Inverted organic solar cells · ZnO nanorods · Electron transport layer · Photovoltaic · Short circuit current density

K. H. Lee · B. Kumar · H.-J. Park · S.-W. Kim
School of Advanced Materials Science and Engineering,
Sungkyunkwan University, Suwon 440-746, Republic of Korea

S.-W. Kim (✉)
SKKU Advanced Institute of Nanotechnology (SAINT)
and Center for Human Interface Nanotechnology (HINT),
Sungkyunkwan University, Suwon 440-746, Republic of Korea
e-mail: kimsw1@skku.edu

Introduction

Organic solar cells (OSCs) have been widely investigated in the past decade due to their numerous potential advantages including relatively inexpensive and light-weight materials, compatibility with flexible plastic substrates, and ease of fabrication [1–3]. However, the short exciton-diffusion length and inefficient exciton dissociation in a polymeric matrix of OSCs results in low quantum efficiency, which limits their use in many potential applications [4, 5]. Moreover, the lifetimes of OSC devices are short, and thus careful encapsulation strategies should be developed for use in practical working environments [6–8]. For the efficient dissociation of excitons, a bulk heterojunction (BHJ) blend of donors and acceptors is generally used, leading to nanoscale morphology and facilitating charge transport in interpenetrating networks [8–10].

In the conventional structure of an OSC based on BHJ, indium tin oxide (ITO) modified with p-type poly(3, 4-ethylene dioxythiophene):(polystyrene sulfonic acid) (PEDOT:PSS) is used as an anode [11]. However, PEDOT:PSS is an acidic water-based solution, which causes interface instability in the photoactive layer and corrosion of the ITO [11, 12]. To improve the interface stability and prevent device degradation, an alternative is to use as an inverted configuration [13], with ITO serving as the cathode and a high work function metal as the anode. It should be pointed out that only modified ITO can serve as the cathode for electron extraction, and thus the functional layers for modifying ITO mainly focus on metal oxides. ZnO is one of the applicable functional metal oxides for use in this application due to its high electron mobility and high degree of transparency in the visible wavelength range. Moreover, its crystal structure allows it to be grown anisotropically, making possible the production of highly

efficient OSCs based on vertically oriented ZnO nanorods (NRs) for use as continuous electron transport pathways [14, 15].

Herein, we report a dramatic increase in the power conversion efficiencies (PCE) of flexible inverted OSCs (IOSCs) fabricated with ZnO NRs/ZnO seed layers acting as direct electron transport pathways. This method involves the growth of ZnO NRs via an aqueous solution route at the low temperature of 90°C. This is a simple and effective process for improving the PCE of IOSCs. Compared with ZnO seed layer-based IOSCs, the PCE of the IOSCs fabricated with ZnO NRs was increased by approximately threefold using simulated air mass (AM) 1.5 global full-sun (1.5G, 100 mW/cm^2) illumination. This work suggests a method to fabricate efficient photovoltaic (PV) devices with larger interface areas for effective exciton dissociation area and optimum continuous carrier transport paths, which should be useful for future applications.

Experimental Section

We first prepared a ZnO seed solution using zinc acetate dihydrate [$Zn(CH_3COO)_2\cdot2H_2O$] as a source and ethanol as a solvent. Briefly, zinc acetate dihydrate (final concentration 30 mM) was stirred for 30 min in ethanol at 60°C. ZnO seed layers were then deposited using spin coating at 3,000 rpm for 30 s onto ITO-coated polyethersulphone (PES) substrates. Spin coating was repeated between 12 and 18 times in order to control ZnO seed layer thickness and density. The deposited seed layers were thermally treated at 150°C for 10 min after each deposition. After seed layer formation, the substrates were maintained in a solution consisting of deionized water, 25 mM zinc nitrate hexahydrate [$Zn(NO_3)_2\cdot6H_2O$], and 25 mM hexamethylenetetramine [$C_6H_{12}N_4$] (HMT) for 30 min at 90°C to prepare the ZnO NRs.

We prepared a P3HT: PCBM-blended solution for active layer deposition using spin coating at 2,000 rpm for 120 s. Poly(3-hexylthiophene) (P3HT) and [6,6]-phenyl C_{61} butyric acid methyl ester (PCBM) were dissolved in chlorobenzene at a weight ratio of 1:1 for 1 day, resulting in a P3HT:PCBM blend. After annealing an active layer for 30 min at 150°C, a 20-nm-thick MoO$_x$ electron blocking layer and a 100-nm Au layer were deposited via thermal evaporation through a shadow mask.

The structure of the IOSCs consisted of Au/MoO$_x$/P3HT:PCBM/ZnO, a NR/ZNO seed layer, and ITO/PES stacked from bottom to top. Investigation into surface morphology and thickness was carried out using field emission scanning electron microscopy (FE-SEM). PV performance was evaluated by measuring short circuit current density (J_{sc}), open circuit voltage (V_{oc}), fill factor (FF), power conversion efficiency (PCE) and series resistance(R_s) using a solar simulator under AM 1.5G conditions (100 mW/cm^2).

Results and Discussion

The cross-sectional FE-SEM images depicted in Fig. 1 show the typical surface morphologies of the ZnO NRs grown on (a) 12 times, (b) 15 times, (c) 18 times deposited ZnO seed layers using spin coating. The thickness of the ZnO seed layer was increased by repeating the spin coating process. The ZnO seed layers were porous and consisted of nanoparticles with a typical diameter of 5 nm. The thicknesses of the seed layers were 115, 130, and 145 nm after 12, 15, and 18 spin coating depositions, respectively. The ZnO NRs were vertically arrayed on the ZnO seed layer with a typical diameter of 30 nm and a length of 250 nm.
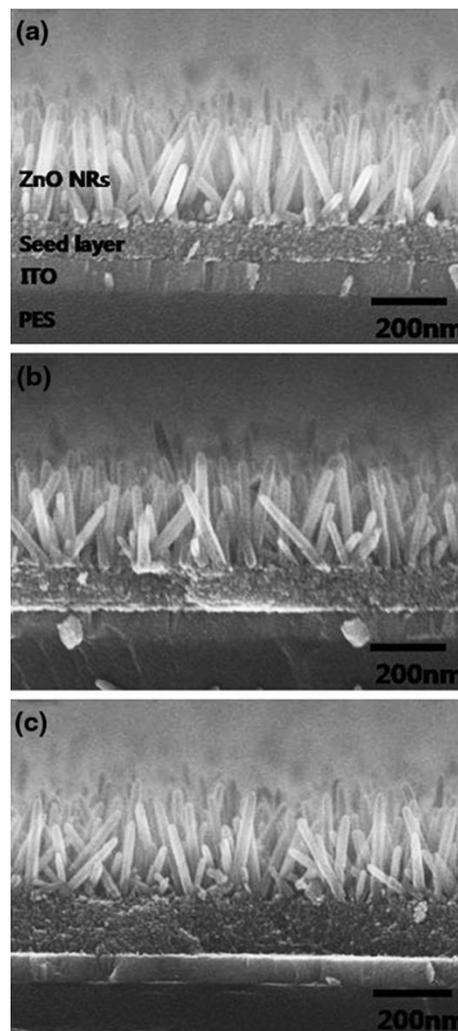

Fig. 1 FE-SEM images of ZnO NRs grown on a ZnO seed layer spin coated onto a PES substrate **a** 12 times, **b** 15 times, **c** and 18 times
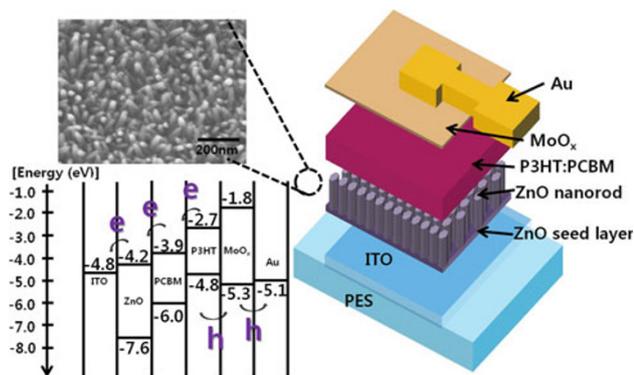
Fig. 2 Device structure and energy diagram of IOSC with ZnO NRs

Fig. 3 Current density voltage (J–V) characteristic for solar cells under AM 1.5 G simulated solar illumination

We fabricated a series of devices with different ZnO seed layer thickness by controlling the number of spin coating depositions. To investigate the role of the ZnO NRs alone, we also fabricated IOSCs with ZnO NRs at the same ZnO seed layer positions. Figure 2 shows the schematic diagram of flexible IOSC and its energy band configuration. The ZnO NRs and seed layer acted as an electron transport layer, while the MoO_x layer acted as a hole transport layer.

Fig. 3 shows the current density–voltage (J–V) characteristics for the solar cells fabricated with/without ZnO NRs by varying the ZnO seed layer thickness. Measurements were carried out under solar-simulated AM 1.5 G illumination with a 100 mW/cm^2 light source. The J_{sc}, V_{oc}, FF, and PCE derived from J–V curves are summarized in Table 1. We found that PV performance improved as seed layer thickness increased for the IOSCs fabricated with the ZnO seed layer, up to an optimum thickness of 130 nm. In IOSC structures, the electron transport layer is affected by injection of holes from the highest occupied molecular orbital (HOMO) level of P3HT—4.8 eV to ITO—4.8 eV [16]. Therefore, to prevent contact between the active layer and the ITO electrode, the ZnO seed layer should exist as a stable compact film. However, the ZnO seed layer was a porous film consisting of nanoparticles and could not completely prevent contact between the organic active layer and the ITO electrode until it reached an optimized
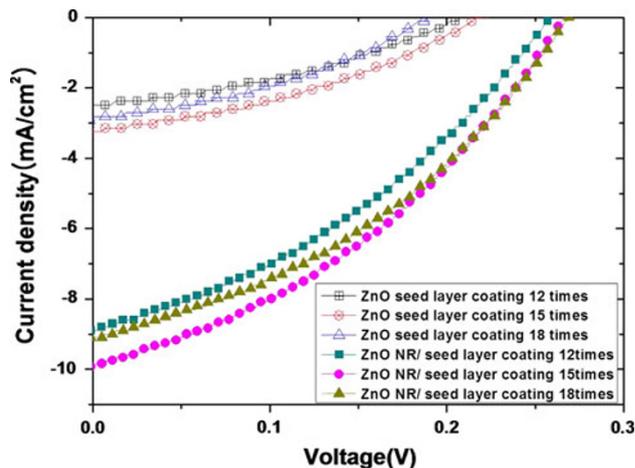
thickness. On the other hand, resistance of the seed layer increased with increasing thickness. As a result, the J_{sc} of the device increased up to the optimum film thickness, after which it began to decrease due to a larger series resistance, as shown in Fig. 3. Consequently, the PV performance of the device varied in the same way. Thus, an optimization process was necessary with respect to the thickness of the electron transport layer in order to prevent contact between the active layer and the ITO electrode with the lowest series resistance. We optimized the seed layer thickness to 130 nm, which allowed for the extraction of the maximum efficiency from the device. Furthermore, we studied the PV performances of IOSCs fabricated with a ZnO seed layer and with a ZnO NRs/ZnO seed layer.

We also compared IOSCs with a ZnO NRs/ZnO seed layer with IOSCs consisting of a ZnO seed layer only. As summarized in Table 1, the PV performance of the IOSCs fabricated with a ZnO NRs/ZnO seed layer was improved about threefold compared with that of IOSCs fabricated with a ZnO seed layer. This substantial improvement in PV performance can be explained in two ways. First, improvement in PV performance was the result of an increased exciton dissociation interface area between ZnO and the active layer using ZnO NRs. The energy level

Table 1 Summary of device performance

| Devices	ZnO seed layer thickness (nm)	J_{sc} (mA/cm^2)	V_{oc} (V)	FF (%)	PCE (%)
ZnO seed layer 12 times	115	2.492	0.211	36.637	0.193
ZnO seed layer 15 times	130	3.250	0.220	36.212	0.259
ZnO seed layer 18 times	145	2.817	0.200	36.308	0.205
ZnO NRs/ZnO seed layer 12 times	250/115	8.900	0.259	35.955	0.829
ZnO NRs/ZnO seed layer 15 times	250/130	9.917	0.266	37.126	0.979
ZnO NRs/ZnO seed layer 18 times	250/145	9.100	0.269	37.971	0.930
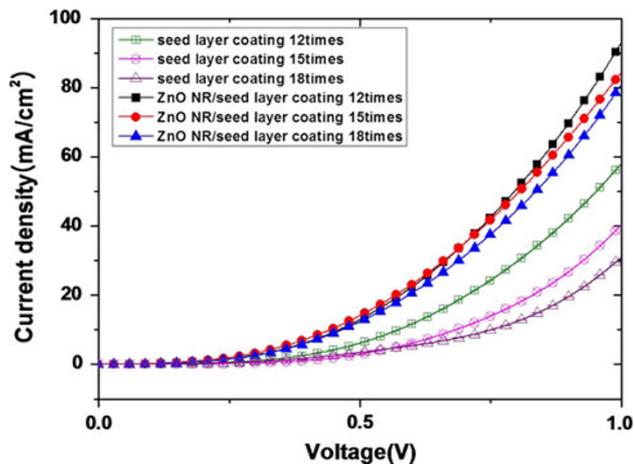
Fig. 4 Dark current density voltage (J–V) curves for IOSCs

diagram in Fig. 2 shows the position of the lowest unoccupied molecular orbital (LUMO) level of ZnO at—4.2 eV [17], which suggests that electrons from P3HT with a LUMO of—2.7 eV [16] can be injected into the ZnO NRs. Therefore, a larger area between ZnO and the active layer is favorable for increased exciton diffusion and separation events. For IOSCs with a ZnO seed layer, the exciton dissociation interface between the ZnO seed layer and organic material was planar, and most of the photo generated excitons were unable to reach the interface. This resulted in a large recombination probability in locations distant from the interface due to low exciton-diffusion length. Conversely, for the IOSCs with a ZnO NRs/ZnO seed layer, upon filling the space between the ZnO NRs with organic materials, the exciton dissociation interface area was greatly increased, and most of the photogene rated excitons were able to reach the interface before recombination.

A second possible reason is a higher mobility of the ZnO NRs. High carrier mobility causes low series resistance (R_s), which increases the efficiencies of solar cells [18]. Because the series resistance in a solar cell contributes to the bulk conductivity of each of the functional layers and the contact resistance between them, and because high charge carrier mobility is beneficial to obtaining a low R_s [19], the lower R_s of the IOSCs with the ZnO NR/ZnO seed layer may reflect improved electron mobility. As demonstrated in previous studies [4, 20], the carrier mobility of ZnO NR is several orders of magnitude larger than that of organic materials due to the occurrence of a hopping mechanism in the organic materials [21]. Therefore, we speculate that the dark current density in IOSCs with a ZnO NRs/ZnO seed layer as a direct pathway for photo-generated electrons was increased compared with that of IOSCs with a ZnO seed layer. Figure 4 shows the J–V curves obtained for the IOSCs with a ZnO NRs/ZnO seed layer

and a ZnO seed layer under forward bias in the dark. The current density of the IOSCs fabricated with ZnO NRs was increased compared with that of IOSCs fabricated with a ZnO seed layer, providing additional evidence for the improvement in PV performance due to the introduction of ZnO NRs.

Conclusions

PV performance of flexible IOSCs with an active layer consisting of a blend of P3HT:PCBM was investigated by varying the thicknesses of ZnO seed layers and by introducing ZnO NRs. A ZnO seed layer or ZnO NRs grown on the seed layer were used as an electron transport layer and pathway to optimize PV performance. The optimized device with ZnO NRs exhibited a threefold increase in PV performance compared with that of a device consisting of a ZnO seed layer without ZnO NRs. The optimization of the electron transport layer in the present work is one of the most important aspects for further improvement on solar cell efficiency.

References

1. W.L. Ma, C.Y. Yang, X. Gong, K. Lee, A.J. Heeger, Thermally Adv. Funct. Mater. **15**, 1617 (2005)
2. M. Reyes-Reyes, K. Kim, D.L. Carroll, Appl. Phys. Lett. **87**, 083506 (2005)
3. F.C. Krebs, Sol. Energy Mater. Sol. Cells **93**, 394 (2009)
4. W.B. Chen, H.F. Xiang, Z.X. Xu, B.-P. Yan, V.A.L. Roy, C.M. Che, Appl. Phys. Lett. **91**, 191109 (2007)
5. M.Y. Chan, S.L. Lai, M.K. Fung, C.S. Lee, S.T. Lee, Appl. Phys. Lett. **90**, 023504 (2007)
6. G. Dennler, C. Lungebschmied, H. Neugebauer, N.S. Sariciftci, M. Latre'che, G. Czeremuskin, M.R. Wertheimer, Thin Solid Films **349**, 511 (2006)
7. J. Fahlteich, M. Fahland, W. Schönberger, N. Schiller, Thin Solid Films **517**, 3075 (2009)
8. D. Chirvase, J. Parisi, J.C. Hummelen, V. Dyakonov, Nanotechnology **15**, 1317 (2004)
9. H. Hoppe, M. Niggemann, C. Winder, J. Kraut, R. Hiesgen, A. Hinsch, D. Meissner, N.S. Sariciftci, Adv. Funct. Mater. **14**, 1005 (2004)

10. H. Hoppe, N.S. Sariciftci, J. Mater. Chem. **16**, 45 (2006)
11. M. Jorgensen, K. Norrman, F.C. Krebs, Sol. Energy Mater. Sol. Cells **92**, 686 (2008)
12. L.M. Chen, Z.R. Hong, G. Li, Y. Yang, Adv. Mater. **21**, 1434 (2009)
13. D.C. Olson, J. Piris, R.T. Collins, S.E. Shaheen, D.S. Ginley, Thin Solid Films **496**, 26 (2006)
14. D.C. Olson, Y.J. Lee, M.S. White, N. Kopidakis, S.E. Shaheen, D.S. Ginley, J.A. Voigt, J.W.P. Hsu, J. Phys. Chem. C **111**, 16640 (2007)
15. D.C. Olson, S.E. Shaheen, R.T. Collins, D.S. Ginley, J. Phys. Chem. C **111**, 16670 (2007)
16. T. Yamanari, T. Taima, J. Sakai, K. Saito, Sol. Energy Mater. Sol. Cells **93**, 759 (2009)
17. L.J.A. Koster, W.J.V. Strien, W.J.E. Beek, P.W.M. Blom, Adv. Funct. Mater. **17**, 1297 (2007)
18. S.E. Shaheen, D.S. Ginley, G.W. Jabbour, MRS Bull. **30**, 10 (2005)
19. H.L. Yip, S.K. Hau, N.S. Baek, H. Ma, A.K.-Y. Jen, Adv. Mater. **20**, 2376 (2008)
20. Z.Y. Zhang, C.H. Jin, X.L. Liang, Q. Chen, L.-M. Peng, Appl. Phys. Lett. **88**, 073102 (2006)
21. P. Sullivan, T.S. Jones, A.J. Ferguson, S. Heutz, Appl. Phys. Lett. **91**, 233114 (2007)